Supporting Information for

Crystal Structure of Poly(trimethylene 2,5-furandicarboxylate) Redux - a new model supported by computational spectroscopy

Catarina F. Araujo[♫], Simão V. Pandeirada[♫], Inês M. Oliveira[♫], Guilherme Rosa[♫], Beatriz Agostinho[♫], Armando J. D. Silvestre[♫], Andreia F. Sousa[♫,♭], Svemir Rudić[♯], Pedro D. Vaz[♪], Mariela M. Nolasco[,♫], Paulo Ribeiro-Claro[♫]*

[♫]CICECO, Departamento de Química, Universidade de Aveiro, Aveiro, Portugal

[♭]Centre for Mechanical Engineering, Materials and Processes, Department of Chemical Engineering, University of Coimbra Rua Sílvio Lima – Polo II, 3030-790 Coimbra, Portugal

[♯]ISIS Neutron & Muon Source, STFC Rutherford Appleton Laboratory, Didcot, United Kingdom

[♪]Champalimaud Foundation, Champalimaud Centre for the Unknown, Lisboa, Portugal

Contents:

NMR analysis

Molecular weight determination

INS spectroscopy in a nutshell

The computational spectroscopy approach

Thermodynamic properties from CASTEP

Supplemental Figures:

Figure S1. PTF ^{1}H-NMR spectrum with the respective carbon resonances.

Figure S2. PTF ^{13}C-NMR spectrum with the respective carbon resonances.

Figure S3. Observed and estimated INS intensities for crystalline PTF calculated at the B3LYP, B3LYP-D3 and M06-2X levels.

Figure S4. Observed infrared intensities for semi-crystalline (PTF-SC, black line) and amorphous (PTF-AM, red line) samples of PTF. Estimated infrared spectra for PTF oligomers establishing intermolecular interactions (*ss-tggt* C-H…O, green line) and an isolated PTF oligomer (*ss-tggt* free, blue line).

Figure S5. Observed INS intensities, as collected using the TOSCA instrument, of an amorphous sample of PTF (black) and estimated INS intensities of PTF oligomers in different conformations, computed at the B3LYP/6-311G(d,p) level. **Figure S4.** Debye Temperature of the PTF crystal as computed using CASTEP.

Figure S6. Variation of the Debye Temperature of the PTF crystal in the 15-1000K temperature range, estimated using CASTEP.

Figure S7. Variation of Entropy, Enthalpy and Gibbs free energy of the PTF crystal in the 15-1000K temperature range, estimated using CASTEP.

Figure S8. Variation of the Lattice Heat Capacity of the PTF crystal in the 15-1000K temperature range, estimated using CASTEP.

Supplemental Data:

Optimized crystal structure coordinates of PTF resulting from CASTEP calculations, with and without constraints, based on *ss-tggt* and *ss-gtgt* conformations.

NMR analysis

^{1}H and ^{13}C nuclear magnetic resonance spectroscopy (^{1}H and ^{13}C-NMR) analyses of samples dissolved in $CDCl_3$ and few drops of TFA were recorded using a Bruker AMX 300 spectrometer, operating at 300 MHz. All chemical shifts were expressed in parts per million (ppm) using $CDCl_3$ as the internal reference.

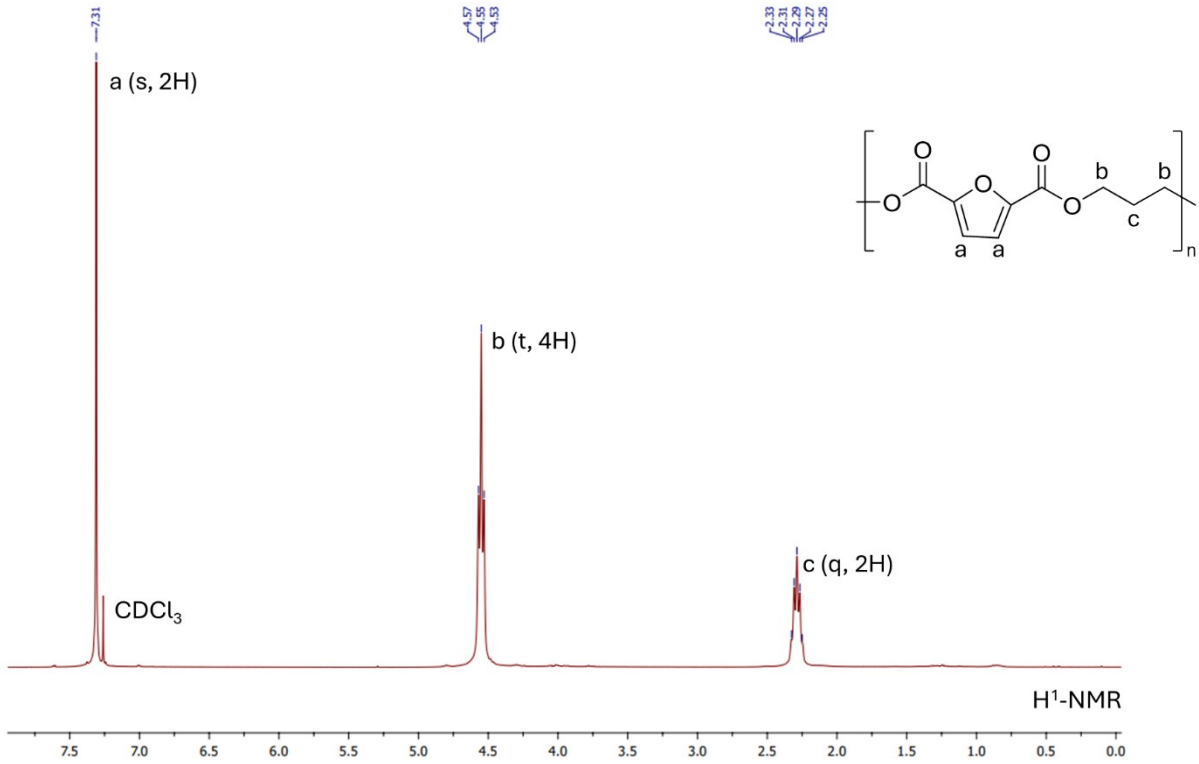

Figure S1. PTF ^{1}H-NMR spectrum with the respective proton resonances.

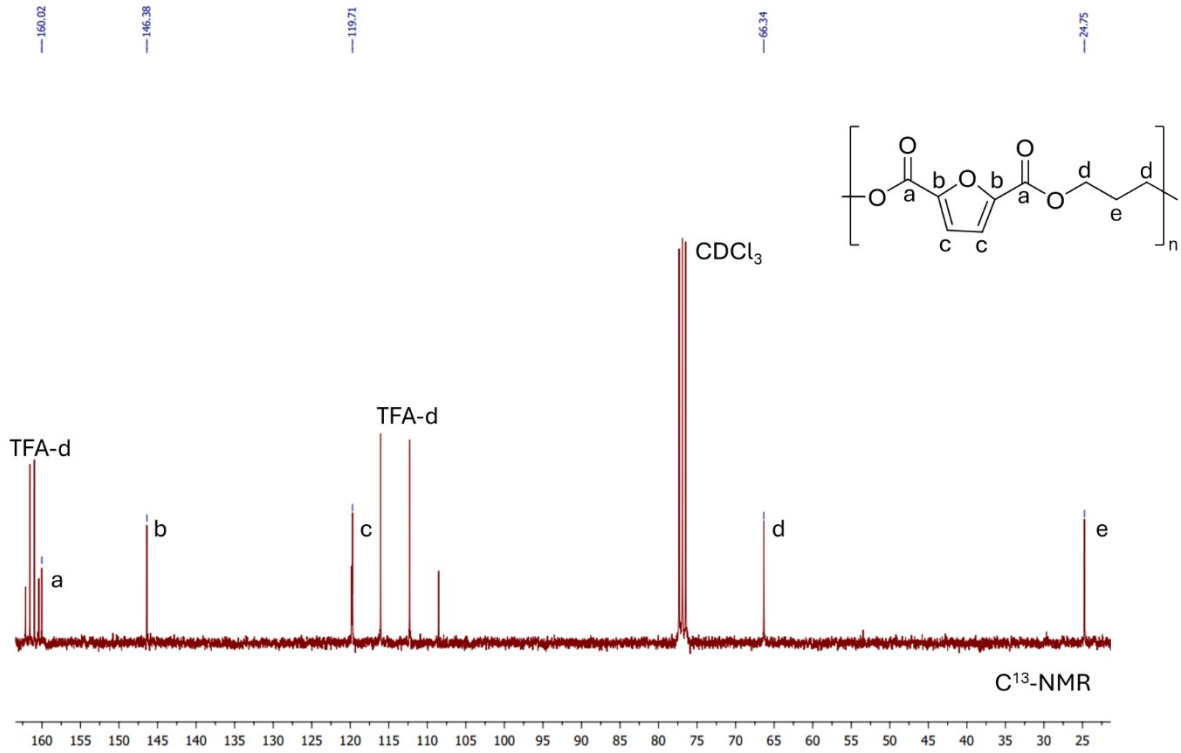

Figure S2. PTF ^{13}C-NMR spectrum with the respective carbon resonances.

Molecular weight determination

Molecular weights were obtained through gas permeation chromatography (GPC) using a 1260 Infinity II High-Temperature GPC system (Agilent Technologies). The separation was carried out using two PL HFIPgel 300 mm columns at 35 ºC. A chloroform/hexafluoro-2-propanol solution (96/4 v/v) was used as the eluent, with a 0.3 ml/min flow rate, and sample concentration of 3mg/ml. The molecular weight was calculated using a conventional calibration curve generated from Polystyrene standards (Agilent Technologies, Mw= 435 – 364 700 g/mol).

Table S1 Number average molecular weight (M_n), weight average molecular weight (M_w) and polydispersity index (M_w/M_n) of PTF as obtained by gas permeation chromatography.

Polymer	M_n (g.mol^{-1})	M_w (g.mol^{-1})	M_w/M_n
2,5-PTF	6726	18162	2.7

INS spectroscopy in a nutshell

INS spectroscopy provides a unique assessment of the structural dynamics of hydrogenous materials that is not amenable from its optical counterparts, infrared and Raman spectroscopies, as it is not constrained by symmetry-related selection rules [1,2].

In INS, the intensity of each fundamental vibrational transition is expressed, for a given atom, by the dynamic structure factor

$$S_i^*(Q,n\nu_k) \propto \frac{(QU_i)^{2n}}{n!}.\sigma.\, exp\left(-Q^2\alpha_i^2\right)$$

where Q ($Å^{-1}$) is the momentum transferred to the sample, n is the quanta involved (n = 1 for fundamental modes), ν_k is the energy of a vibrational mode, U_i (Å) is the displacement vector of atom i in mode k, σ is the neutron scattering cross section of atom i and α_i (Å) is related to a mass-weighted sum of the displacements of the atom in all vibrational modes, a term whose magnitude is in part determined by the thermal motion of the molecule [1,2].

The momentum dependence arises because a neutron has mass (1.009 amu) and any scattering event will involve a change in momentum (since the neutron will change direction) and may also involve a change in energy. The dependence of intensity on Q is the major difference between INS and optical (infrared and Raman) spectroscopies, where vibrational modes are observed at (nearly) zero momentum transfer (Q = 0).

This means that in INS the intensity of a band associated with a given vibrational mode is proportional to the neutron scattering cross section of the moving nuclei and to the amplitude of nuclei displacement. While the former is a physical property of the nuclei, the latter is readily obtained from DFT calculations (frequency, or phonon, calculations).

1. Mitchell, P.C.H.; Parker, S.F.; Ramirez-Cuesta, A.J.; Tomkinson, J. *Vibrational Spectroscopy with Neutrons: With Applications in Chemistry, Biology, Materials Science and Catalysis*; Finney, J.L., Worcester, D.L., Eds.; World Scientific Publishing Co: Singapore, 2005; ISBN 978-981-256-013-1.
2. Parker, S.F.; Ramirez-Cuesta, A.J.; Daemen, L. Vibrational spectroscopy with neutrons: Recent developments. *Spectrochim. Acta Part A – Mol. Biomol. Spectrosc.* **2018**, *190*, 518–523.

The computational spectroscopy approach

Computational spectroscopy aims at obtaining a reliable computational description of the experimental spectrum (in this work, the vibrational spectrum). A good agreement between calculated and experimental spectra validates the theoretical model and supports data analysis and interpretation.

Currently, there is no quantitative measure to assess the similarity between experimental and calculated spectra (the use of machine learning algorithms for pattern recognition is discussed, but not yet widely available). Therefore, the comparison relies on visual inspection and qualitative evaluations ranging from “reasonable” to “excellent”.

In Figure S3 below, the description of the experimental INS spectrum obtained from a discrete frequency calculation on a PTF dimer that mimics the crystal motif, ran at three different levels of theory, can be classified as “very good” for all cases. The resemblance between observed and estimated spectra is especially impressive when one considers that a) the discrete model used only includes C-H···O bonds between two adjacent PTF oligomers, which is akin to a small fragment of the vast 2D sheets found in the crystal, with no representation of π-π interactions due to the absence of vertical stacking and b) the experimental spectrum refers to a semi-crystalline sample, where crystalline domains co-exist with amorphous regions. In particular, the description of the band profile in the 400-800 cm^{-1} region is clearly “excellent” at all levels, while the description of the region above 1200 cm^{-1} shows only "generally good" agreement in terms of band intensities, with B3LYP slightly better in terms of band positions.

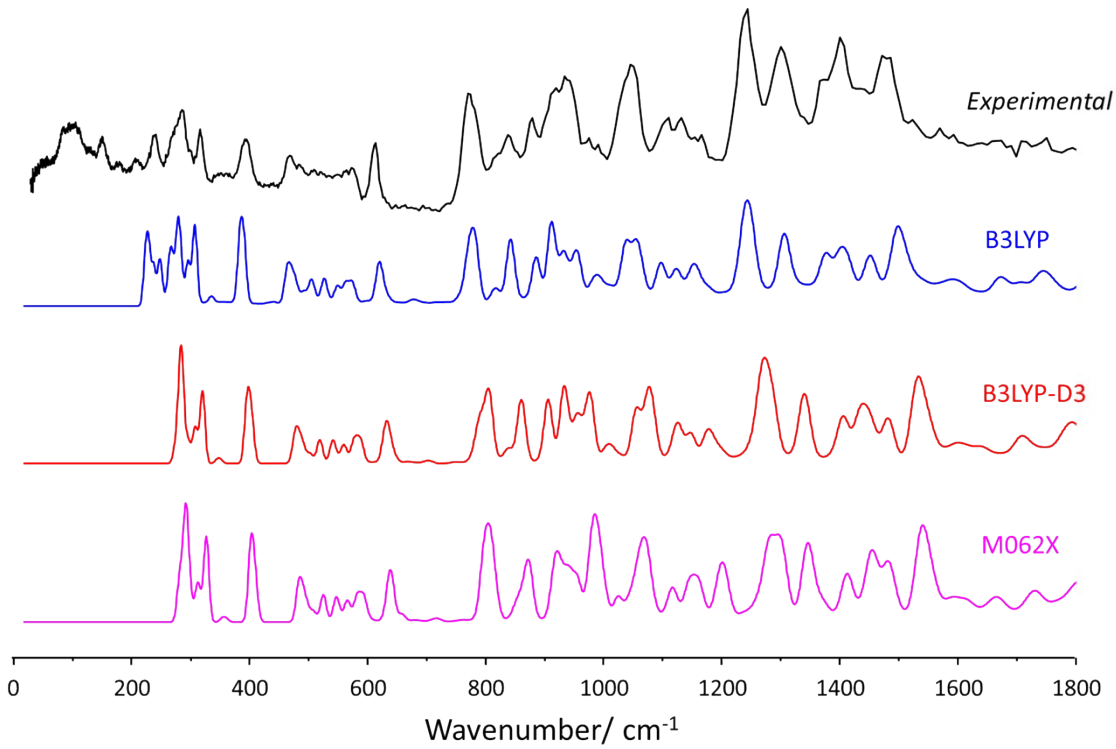

Figure S3. Observed and estimated INS intensities for a discrete model of crystalline PTF calculated at the B3LYP, B3LYP-D3 and M06-2X levels.

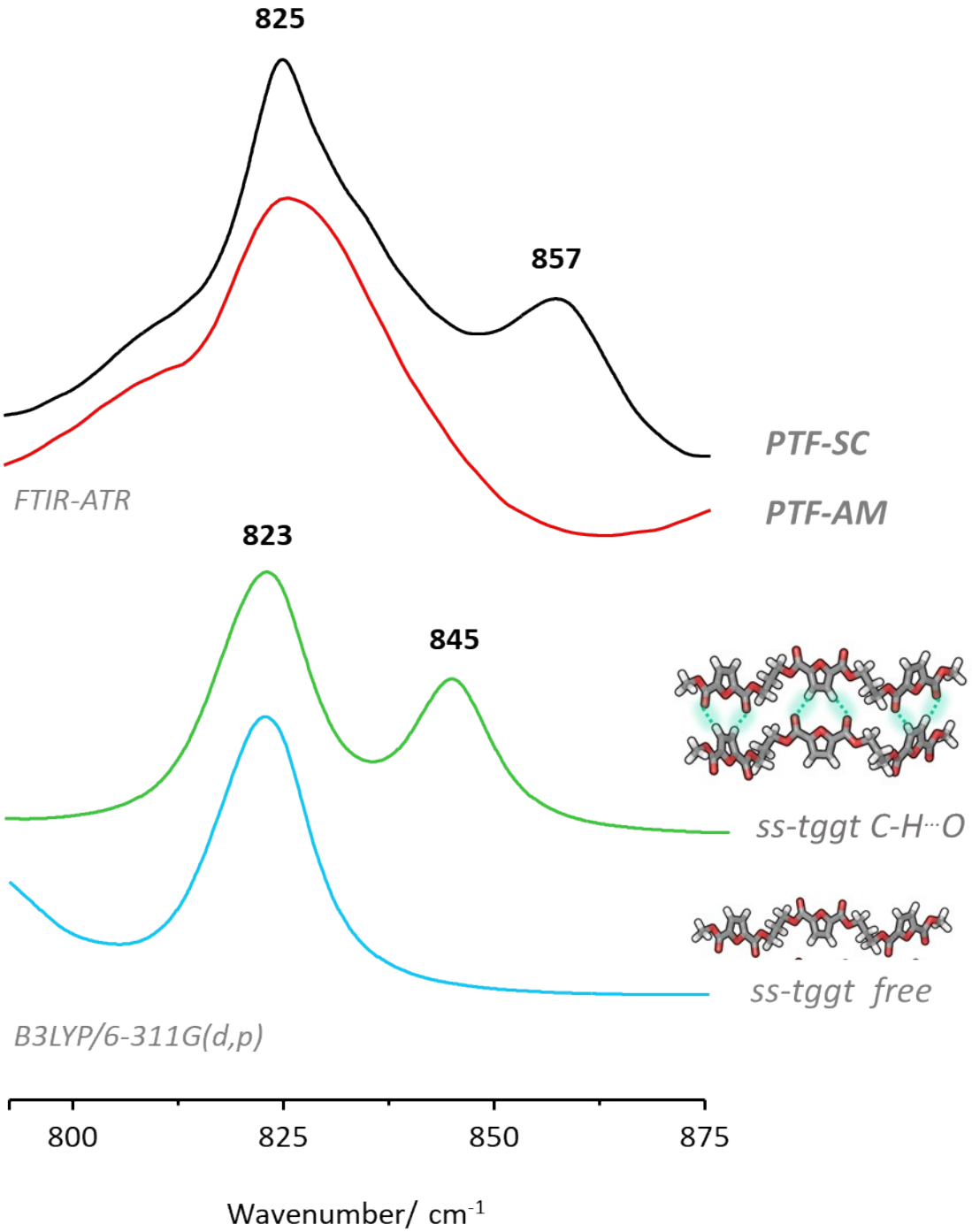

Figure S4. Observed infrared intensities for semi-crystalline (PTF-SC, black line) and amorphous (PTF-AM, red line) samples of PTF. Estimated infrared spectra for PTF oligomers establishing intermolecular interactions (*ss-tggt* C-H…O, green line) and an isolated PTF oligomer (*ss-tggt* free, blue line).

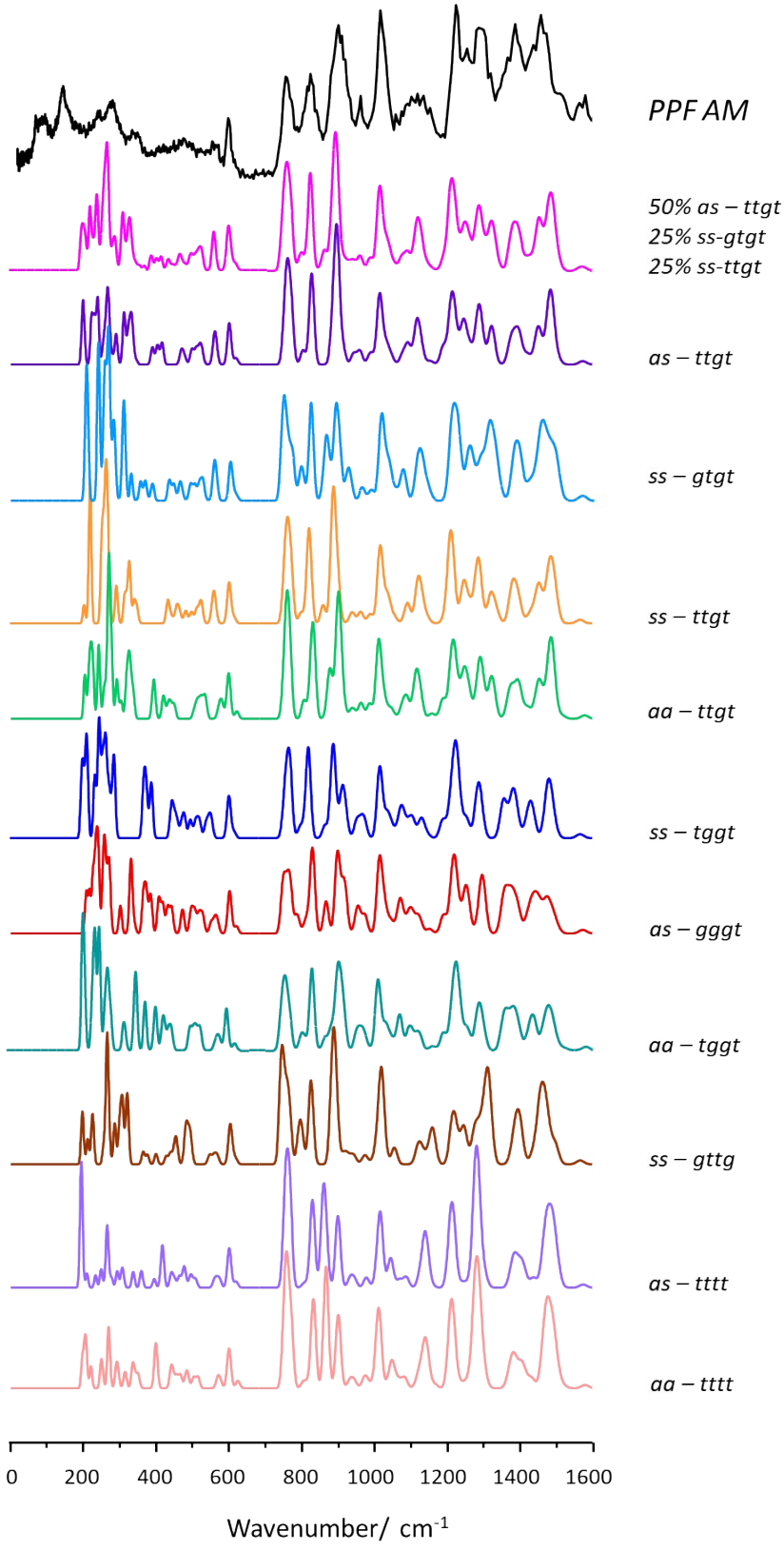

Figure S5. Observed INS intensities, as collected using the TOSCA instrument, of an amorphous sample of PTF (black) and estimated INS intensities of PTF oligomers in different conformations, computed at the B3LYP/6-311G(d,p) level.

Thermodynamic Properties from CASTEP

The phonon density of states calculated using CASTEP can be used to derive thermodynamic properties such as Debye temperature, Gibbs free energy, Enthalpy, Entropy and lattice heat capacity. The variation with temperature of the aforementioned properties, for the herein proposed crystalline structure of PTF, are shown in Figures S6, S7 and S8. At 298K, the lattice heat capacity of PTF is estimated to be 204 J/mol·K. The lattice heat capacity value estimated herein refers only to the crystalline regions of PTF and is expected to deviate from experimental values measured on semi-crystalline samples, where highly oriented crystalline domains are interspersed with disordered amorphous regions.

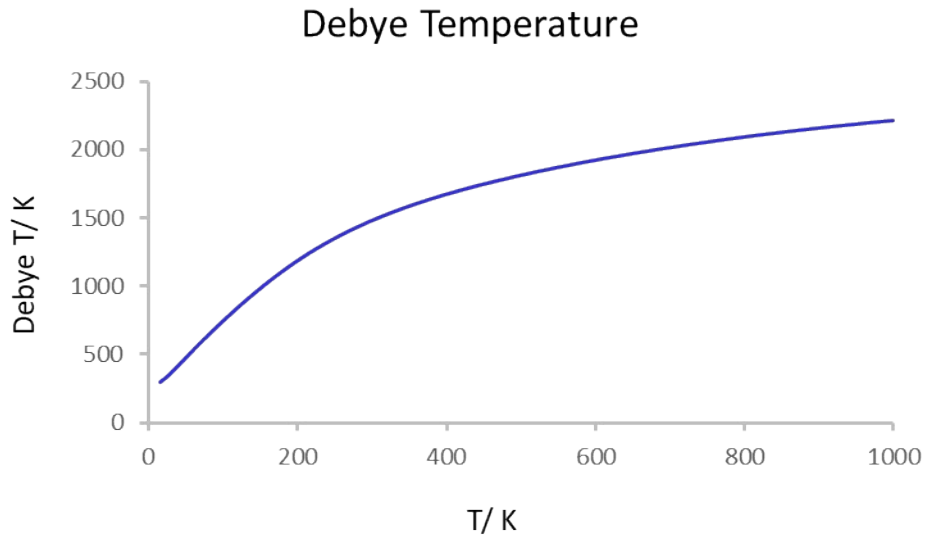

Figure S6. Variation of the Debye Temperature of the PTF crystal in the 15-1000K temperature range, estimated using CASTEP.

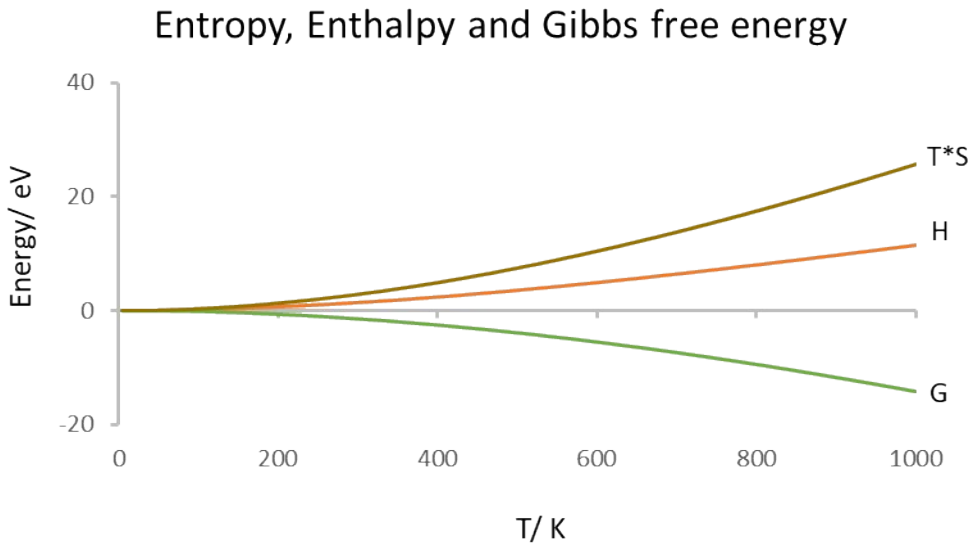

Figure S7. Variation of Entropy, Enthalpy and Gibbs free energy of the PTF crystal in the 15-1000K temperature range, estimated using CASTEP.

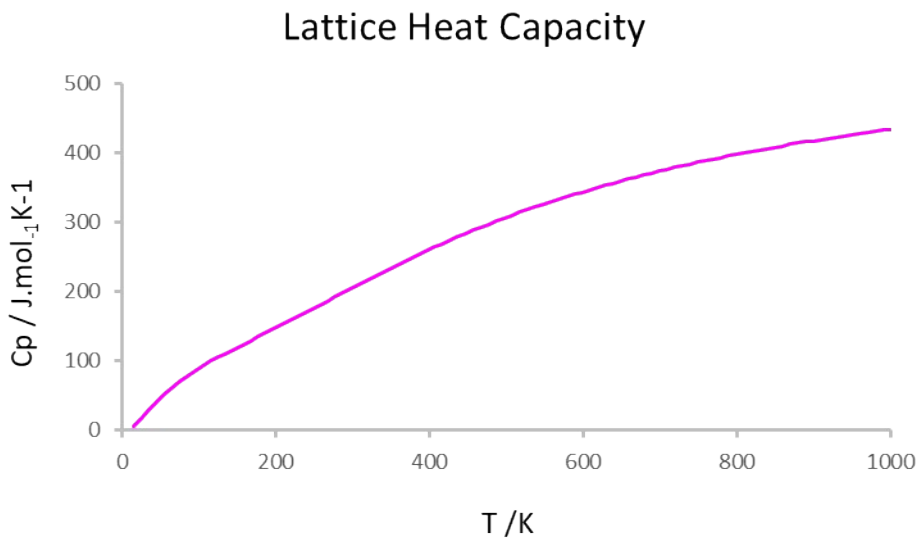

Figure S8. Variation of the Lattice Heat Capacity of the PTF crystal in the 15-1000K temperature range, estimated using CASTEP.

Supplemental data:

Optimized crystal structure coordinates of PTF resulting from CASTEP calculations, with and without constraints, based on *ss-tggt* and *ss-gtgt* conformations.

Crystal structure coordinates resulting from a fully relaxed CASTEP optimization where the input model is based on a *ss-tggt* conformation

_cell_length_a	4.52
_cell_length_b	5.8144
_cell_length_c	16.689
_cell_angle_alpha	90.0000
_cell_angle_beta	90.0000
_cell_angle_gamma	104.59

H	0.275446	0.338590	1.049623
H	-0.155275	0.254708	0.931581
H	-0.848175	-0.404092	0.802634
H	-0.971129	-0.011336	0.786396
H	-0.444016	0.248488	0.763686
H	-0.959561	-0.153154	0.693281
H	-0.717803	0.287052	0.692202
H	-0.144030	-0.175547	0.551870
H	0.279799	-0.098595	0.432270
H	0.963693	0.552207	0.297092
H	1.083637	0.157674	0.282651
H	0.630001	0.452330	0.236752
H	0.554869	-0.101794	0.262997
H	1.067417	0.294694	0.188817
H	0.824004	-0.145157	0.190794
H	-0.518387	-0.306702	0.740557
C	0.199158	-0.051144	1.046148
C	0.160149	0.167804	1.024097
C	-0.062530	0.124441	0.962740
C	-0.143686	-0.118499	0.951115
C	-0.350090	-0.268671	0.893293
C	-0.673605	-0.247700	0.781962
C	-0.817790	-0.065895	0.743433
C	-0.595530	0.160517	0.715271
C	-0.250713	0.291317	0.608195
C	-0.068462	0.214010	0.545878
C	-0.030578	-0.006360	0.525026
C	0.188295	0.033449	0.462829

C	0.268220	0.275323	0.449407
C	0.470933	0.422295	0.390147
C	0.787343	0.395105	0.277857
C	0.928453	0.210634	0.239808
C	0.703192	-0.016845	0.213623
O	0.015137	-0.228507	1.001568
O	-0.378141	-0.480866	0.883046
O	-0.497426	-0.134139	0.850630
O	-0.408879	0.102937	0.650857
O	-0.257478	0.497114	0.620718
O	0.112425	0.388529	0.499680
O	0.497926	0.633957	0.378522
O	0.615471	0.285275	0.347664
C	0.351780	-0.152977	0.108404
O	0.358997	-0.358063	0.122126
O	0.513513	0.037537	0.149449

Crystal structure coordinates resulting from a fully relaxed CASTEP optimization where the input model is based on a *ss-gtgt* conformation

_cell_length_a	5.6720
_cell_length_b	4.5783
_cell_length_c	10.8860
_cell_angle_alpha	123.2038
_cell_angle_beta	107.7524
_cell_angle_gamma	91.9153

O	0.634630	0.568040	0.200670
C	0.440940	0.524270	0.075940
C	0.207230	0.397690	0.066190
C	0.258420	0.361310	0.192120
H	0.120570	0.268900	0.221700
C	0.520990	0.464810	0.269490
C	0.694780	0.478790	0.404810
O	0.927680	0.573430	0.458100
O	0.559120	0.377550	0.464090
C	0.712410	0.380860	0.598870
C	0.534800	0.277250	0.656010
C	0.415180	0.579360	0.748620
O	0.331050	0.521640	0.849350
C	0.524750	0.621070	0.985290
H	0.840880	0.651750	0.693130
H	0.832210	0.191150	0.561120
H	0.653660	0.216830	0.736020
H	0.385400	0.030030	0.556500
H	0.244030	0.586630	0.670460
H	0.554710	0.842300	0.825440
O	0.745210	0.768000	1.026630
H	0.022010	0.350590	-0.017920

Crystal structure coordinates resulting from a CASTEP optimization with fixed cell parameters where the input model is based on a *ss-tggt* conformation

_cell_length_a	5.9000
_cell_length_b	16.6890
_cell_length_c	5.0000
_cell_angle_alpha	90.0000
_cell_angle_beta	104.5850
_cell_angle_gamma	90.0000

H	-0.483950	-0.195920	-0.814670
H	-0.107170	-0.212660	-0.948290
H	-0.382050	-0.260100	-0.522760
H	-0.249350	-0.305290	-0.937580
C	-0.189470	-0.049020	-0.181010
C	-0.336580	-0.109880	-0.355270
C	-0.327430	-0.217950	-0.663460
C	-0.156670	-0.256260	-0.807950
O	-0.540810	-0.123770	-0.360930
O	-0.210180	-0.150170	-0.502770
H	-0.174900	0.438550	0.215410
H	-0.168690	0.261100	0.489290
H	-0.183440	0.186930	0.739980
C	-0.046910	0.467760	0.125380
C	-0.070380	0.213170	0.619080
C	-0.200030	0.107370	0.300270
C	-0.125140	0.047600	0.124330
O	-0.015280	0.151170	0.440090
O	-0.401320	0.116880	0.316820
O	-0.296880	-0.000660	-0.029330
H	-0.255610	0.558290	-0.167870
C	-0.088690	0.530040	-0.073420

Crystal structure coordinates resulting from a CASTEP optimization with fixed cell parameters where the input model is based on a *ss-gtgt* conformation

_cell_length_a	6.1200
_cell_length_b	4.6100
_cell_length_c	11.0700
_cell_angle_alpha	119.0000
_cell_angle_beta	117.0000
_cell_angle_gamma	86.5000

O	0.619560	0.595460	0.218270
C	0.446820	0.514120	0.068810
C	0.223350	0.337310	0.023590
C	0.259990	0.307370	0.152680
H	0.125040	0.182710	0.159810
C	0.505030	0.467110	0.268130
C	0.667880	0.515670	0.425660
O	0.888020	0.657520	0.506780
O	0.544040	0.386680	0.469390
C	0.703500	0.398570	0.618060
C	0.541770	0.299480	0.668670
C	0.425520	0.585910	0.747720
O	0.351410	0.516170	0.840440
C	0.534350	0.623490	0.990760
H	0.819340	0.654630	0.707350
H	0.829990	0.223050	0.599140
H	0.666440	0.230250	0.755530
H	0.396470	0.072140	0.568720
H	0.253120	0.609420	0.662450
H	0.560740	0.828340	0.827500
O	0.743240	0.784780	1.052700
H	0.055050	0.242100	-0.089510